

## Accepted Manuscript

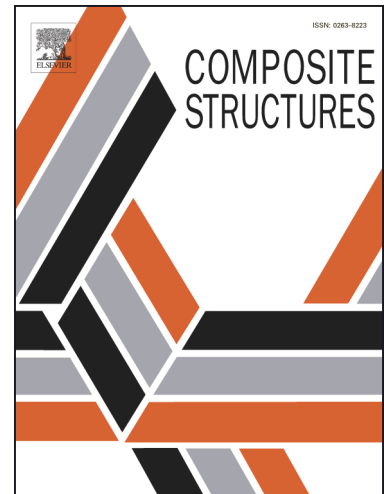
Inline monitoring of basalt-based composites under impact tests

S. Boccardi, N.D. Boffa, G.M. Carlomagno, G. Del Core, C. Meola, P. Russo,  
G. Simeoli

PII: S0263-8223(18)32672-2  
DOI: <https://doi.org/10.1016/j.compstruct.2018.11.038>  
Reference: COST 10403

To appear in: *Composite Structures*

Received Date: 27 July 2018  
Revised Date: 4 October 2018  
Accepted Date: 13 November 2018



Please cite this article as: Boccardi, S., Boffa, N.D., Carlomagno, G.M., Del Core, G., Meola, C., Russo, P., Simeoli, G., Inline monitoring of basalt-based composites under impact tests, *Composite Structures* (2018), doi: <https://doi.org/10.1016/j.compstruct.2018.11.038>

This is a PDF file of an unedited manuscript that has been accepted for publication. As a service to our customers we are providing this early version of the manuscript. The manuscript will undergo copyediting, typesetting, and review of the resulting proof before it is published in its final form. Please note that during the production process errors may be discovered which could affect the content, and all legal disclaimers that apply to the journal pertain.

## Inline monitoring of basalt-based composites under impact tests

S. Boccardi<sup>1,2</sup>, N.D. Boffa<sup>1</sup>, G.M. Carlomagno<sup>1</sup>, G. Del Core<sup>2</sup>, C. Meola<sup>1</sup>, P. Russo<sup>3</sup>, G. Simeoli<sup>3</sup>

<sup>1</sup>Department of Industrial Engineering - Aerospace Division, University of Naples Federico II, Via Claudio, 21, 80125 Napoli, Italy

<sup>2</sup>Department of Science and Technology, University of Naples Parthenope, Centro Direzionale, Isola C4, 80143 Napoli, Italy

<sup>3</sup>Institute for Polymers, Composites and Biomaterials, National Council of Research, Pozzuoli (Na), Italy

### Abstract

Scope of the present work is to visualize with infrared thermography the impact damaging of basalt-based composites. Two types of specimens are prepared with basalt fibres embedded in a polypropylene (PP) matrix, which is used either pure, or modified with the addition of a coupling agent. The latter improves the fibre/matrix interface strength providing in practice a material of different characteristics. Specimens are impacted at low velocity/energy with a modified Charpy pendulum while the infrared camera views the surface opposite to the impacted one and records thermal images in time sequence. The acquired sequences are post-processed to obtain information which may be exploited for the material characterization. In particular, the attention is to identify initiation and propagation of the impact damage and the overall delamination extension, as well as to discriminate likely differences between grafted and un-grafted composites in their impact-reaction. As a main result, the effects of the specimen's fixture on the damage extension are highlighted.

**Keywords:** Basalt-polypropylene composites, Impact damage, Inline monitoring, Infrared thermography

### 1. Introduction

The growing awareness towards the environment is demanding for environmentally friendly materials, so moving the attention from the petrochemical resources towards more natural ones. Within this scenario, basalt fibres are attracting consideration from the scientific community because they seem to be adequate as reinforcement of composites and to comply with the

environment safeguard rules [1]. In fact, basalt is available in nature in volcanic rocks and can be reduced in fibres, which are well suited to be used as reinforcement of both thermoset and thermoplastic matrices to create different types of composite materials. Basalt fibres are ecologically pure and, unlike the conventional asbestos/glass ones, which can cause health hazards, are non-hazardous as they are spun with a diameter higher than 6  $\mu\text{m}$  [2]. In addition, abrasion of basalt only produces thick fibre fragments that pose no respiratory hazard, even if, as with most substances, care in its handling is recommended. Basalt fibres are non-reactive toward water and do not cause air pollution and have a wide spectrum of applications. They are mainly produced for structural and electro-technical purposes including electromagnetic shielding structures, automobiles, aircraft, ships and household appliance components [3-5].

Based on the investigation until now carried out, the obtained composites seem to have good features, which make them comparable, or superior, to the most commonly used ones [1, 2, 6]. It seems that, compared to glass, basalt fibres have higher or comparable modulus and strength [7, 8], high chemo- and thermal stability [8] and good thermal, electrical and sound insulating properties [9]. In particular, the thermal insulating ability of basalt is three times that of asbestos making it suitable for use in fire protection devices [10]. Basalt has much better chemical resistance than glass fibre allowing its use for the production of pipes for the transport of corrosive fluids. It is noteworthy to consider that the replacement of glass fibres with basalt fibres can reduce the risk of environment pollution, the high-toxic metals and oxides (which are released with the production of glass fibres [11]) being eliminated. Therefore, there are many advantages to use basalt fibres for the reinforcement of both polymers and ceramic matrices composites [11, 12].

However, some aspects deserve consideration. Amongst them, there is the poor adhesion between basalt fibres and a polymeric matrix like polypropylene (PP), so requiring a coupling agent such as Polybond (polypropylene-g-maleic anhydride (PP-g-MA)) to enhance interfacial interaction [13]; the latter leading to improvement of the mechanical properties. A better bonding between the matrix and the basalt fibre can also be achieved by hybridizing the surface of fibres with coupling agents like silanes [14]. As reported in the review by Dhand et al. [15] many researchers investigated basalt fibres obtaining promising results, but further investigation is necessary to allow for their broad exploitation in a wide number of applications.

In general, many factors affect the performance of a composite material, demanding for performance assessment through many different tests prior to its introduction on the market. In particular, a material is required to behave differently depending on the specific application sector: aerospace, automotive, naval, or civil engineering and architecture. Therefore, the investigation may be a long way on involving different expertise and instrumentation. Our group, at the University of

Naples Federico II, has been working for years with infrared thermography (IRT) applied to different types of composites, with a twofold function of non-destructive evaluation (NDE) and inline monitoring of mechanical tests (cyclic and quasi-static bending, as well as impact tests); an overview is presented in a recent book [16]. The investigated materials were mostly: carbon/epoxy, glass/epoxy and polypropylene reinforced with either glass, or jute, fibres. The acquired expertise is now directed also towards composites involving basalt fibres. In particular, the intention is to identify initiation and propagation of the impact damage, to evaluate the overall delamination extension, and to discriminate likely differences in the behaviour of basalt fibres when embedded in either a pure PP matrix, or modified with a coupling agent (to improve interface bonding). In other words, the aim is to see whether infrared thermography may help to get new information on the impact damaging of basalt based composites, or at least contribute to validate (verify) previous knowledge.

## 2. Experimental

### 2.1. Description of specimens

Two types of specimens were prepared involving the same reinforcement embedded in two types of matrix. More specifically, the reinforcement is made of a plain weave type woven basalt fibre fabric, with a specific mass of 210 g/m<sup>2</sup>, from Incotology, GmbH. The basic matrix is made of polypropylene Hyosung Topilene PP J640 (MFI@230 °C, 2.16 kg: 10 g/10 min; Songhan Plastic Technology Co. Ltd.), which is used pure (PPB specimens), or modified with the addition of 2 % in weight of Polybond 3000 (PP-g-MA, MFI@190 °C, 2.16 kg: 405 g/10 min; 1.2 % in weight of maleic anhydride, Chemtura, Philadelphia) for the PC2B specimens. As already stated in literature [13], the addition of polypropylene grafted with maleic anhydride (PP-g-MA), enhances bonding between fibres and matrix, getting a material of higher interface strength.

Each specimen includes 18 balanced basalt fabric layers 0°/90° symmetrically arranged with respect to the middle plane of the laminate ( $[(0/90)_9]_s$  configuration), with a basalt fibre content of 50% by volume (the actual relative percentages of fibre and matrix evaluated according to ASTM D 3171-04, Test Method II). Laminates are obtained by alternating layers of polypropylene films and basalt fibre fabrics by the hand lay-up film-stacking technique and with the aid of a compression moulding machine (model P400E, Collin GmbH, Germany) under pre-optimized conditions (Fig. 1). Each specimen is 300 mm x 300 mm with a target thickness of 3 mm.

Specific details of investigated specimens in terms of code, thickness and composition are summarized in the following Table 1.

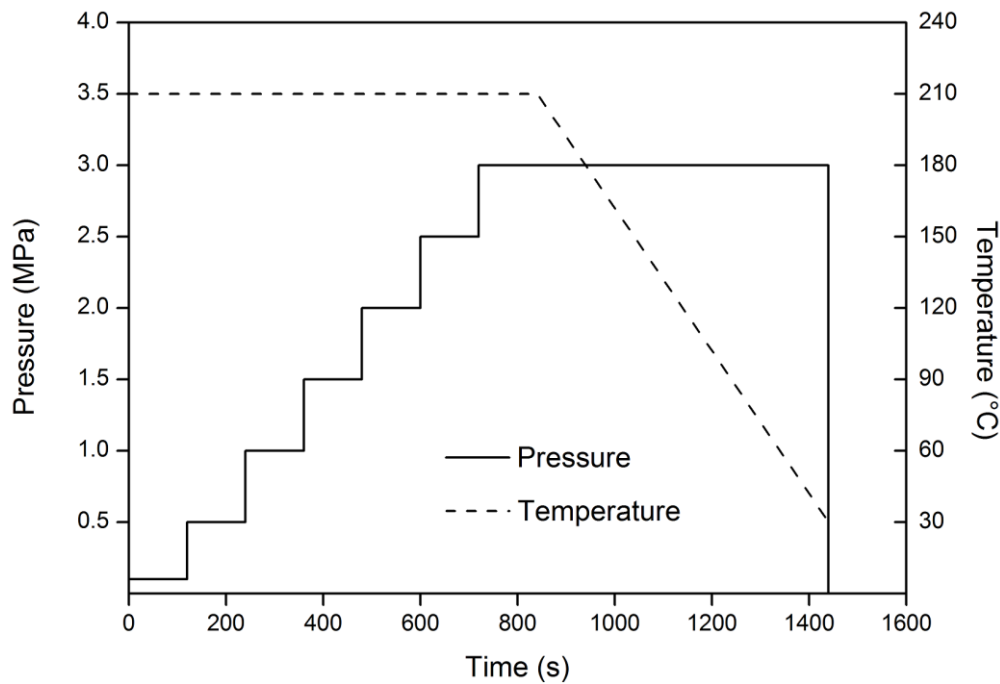


Fig. 1 Compression moulding pressure and temperature against time.

**Table 1 – Investigated specimens**

Code	Thickness (mm)	Composition (Matrix – Reinforcement)
PPB	3.0	Neat PP - Woven basalt fibres
PC2B	3.0	Modified PP (2 wt% PP-g-MA) Woven basalt fibres

## 2.2. Impact tests

Impact tests are carried out with a modified Charpy pendulum with a hemispherical shaped hammer nose, 12.7 mm in diameter. A sketch of the setup is shown in Fig. 2. Each specimen is placed inside a special fixture which includes two large plates, each having a window 12.5 cm x 7.5 cm to allow for the contact with the hammer from one side and optical view (by the infrared camera) from the other one. A small sample of the same material, positioned over one corner of the viewed window, remains unloaded and is used as reference to correct the camera noise. The impact energy is varied between  $E = 5$  and 15 J and is set by suitably adjusting the falling height of the Charpy arm.

The SC6000 infrared camera (Flir systems) is used to acquire sequences of images at 95.5 Hz frame rate during the impact event. In particular, to account for the significant evolution of thermal signatures with respect to the ambient temperature, the acquisition starts few seconds before beginning of the impact and lasts for some time after. In addition, a wide enough area is viewed to allow visualization of any likely interference with the fixture borders; this limits the spatial resolution, which is 0.7 pixel/mm. This value could appear low, but, based on experience and at

least for the used infrared camera, which has high thermal resolution, is enough to evaluate the temperature variations linked with the damage extension. It is worth noting that a high frame rate is necessary to visualize the initial cooling phase which is very fast, while in the present work we are mostly interested in the heating up, which evolves slower.

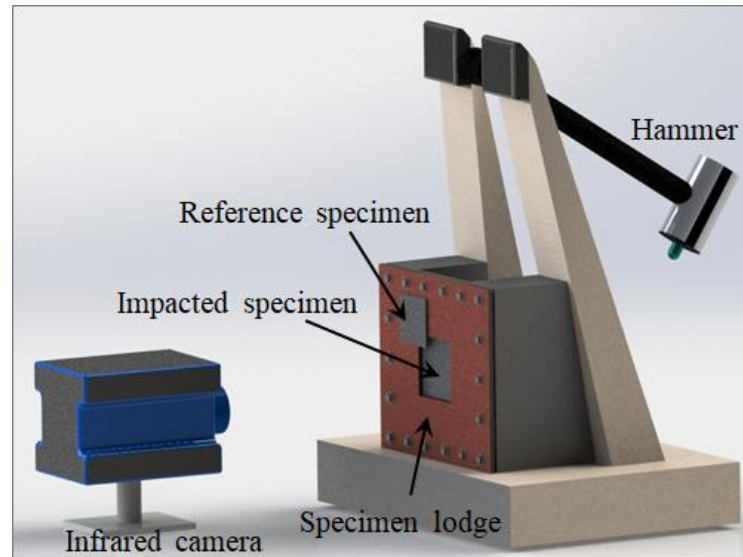


Fig. 2 Sketch of the experimental setup

### 3. Data analysis and discussion

Information on the material behaviour under impact can be derived from the evolution of thermal signatures over time. Any acquired  $T$  thermal images sequence is post-processed to create a sequence of  $\Delta T$  images accounting for temperature variations with respect to the initial unloaded condition:

$$\Delta T(i, j, t) = T(i, j, t) - T(i, j, 0) \quad (1)$$

$i$  and  $j$  representing lines and columns of the surface temperature array,  $t$  the time instant at which images are recorded; more specifically,  $t = 0$  indicates the image of the sequence, before loading, for which the specimen surface is at ambient temperature. Some  $\Delta T$  images, extracted from the  $\Delta T$  sequence created with Eq. 1 of both PPB and PC2B specimens impacted at  $E = 15$  J, are shown in Figs. 3 and 4. As it can be seen, the first image (a) is of almost uniform colour referring to  $\Delta T = 0$  before the impact. Sudden at the impact, a central dark zone appears (b) due to the surface bending under the pushing impactor force. This dark zone, which accounts for the material cooling down (polymer network stretching), is more pronounced for the PC2B specimen. This means that the

improved fibres-matrix interface allows for bending of the laminate through its entire thickness preventing the slipping effect of layers of the PPB weaker bonded configuration. Later on, the dark zone evolves into a cross shaped structure (c) for both specimens, but with the difference that it disappears first over the PC2B specimen. In fact, at  $t = 0.03$  s no dark zones are present on the image (Fig. 4d) of the PC2B specimen, while a dark cross remains still visible on the image (Fig. 3d) of the PPB specimen. This because the better bonded interface of the PC2B specimen is more rigid and promotes early dissipative effects with local heating up as can also be seen by comparing the  $\Delta T$  images of both specimens for increasing the time (e-h).

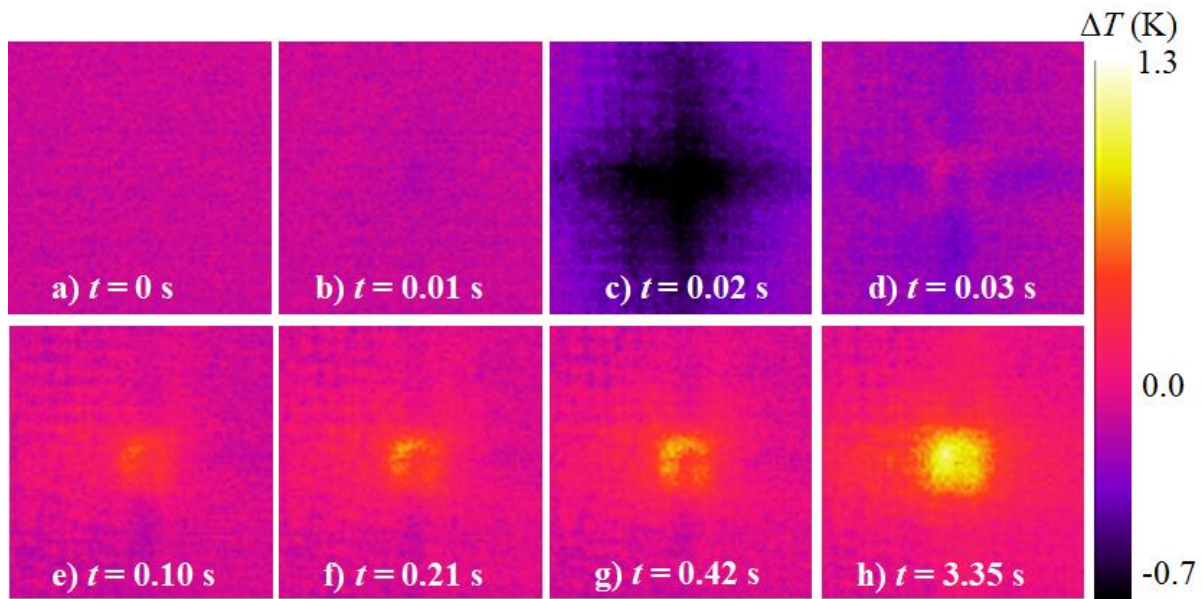


Fig. 3 Some  $\Delta T$  images of the PPB specimen impacted at  $E = 15$  J

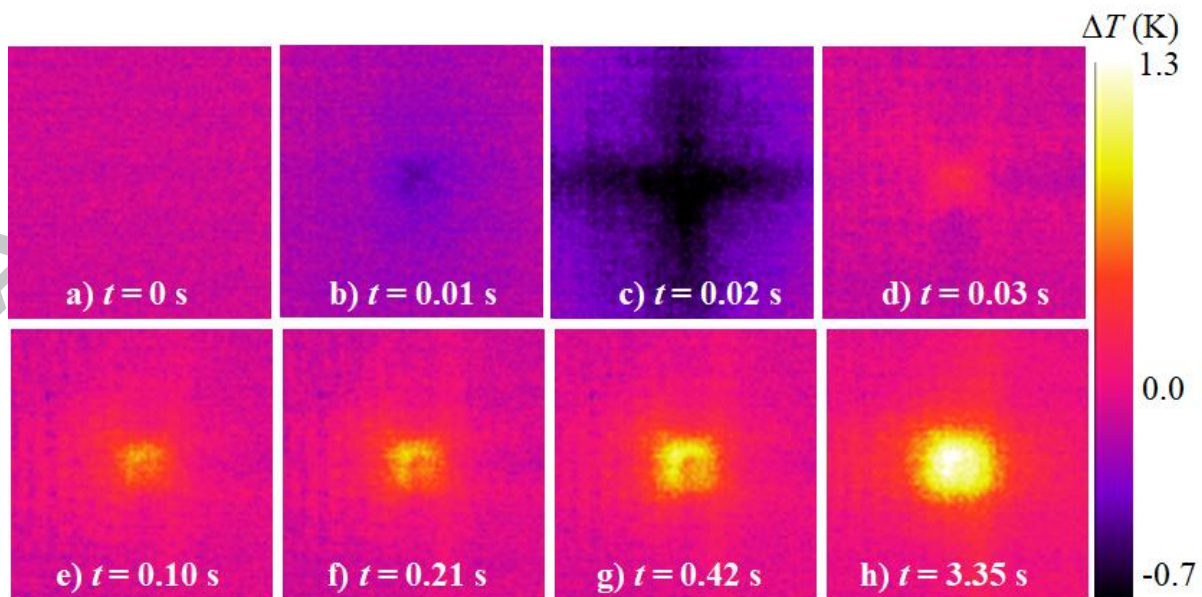


Fig. 4 Some  $\Delta T$  images of the PC2B specimen impacted at  $E = 15$  J

On the whole, the cooling down indicates that the viewed surface (opposite to the impacted one) is under tension due to the impact pushing force and is undergoing volume variation linked to thermo-elastic effects [17, 18]. Instead, the heating up is due to dissipation of the energy absorbed by the specimen (thermo-plastic effect). The cold and hot stains assume a geometrical shape, which, amongst others, is driven by the material type, stacking sequence (layers disposition and orientation) and the fixture geometry. The latter somehow affects the warm area distribution and will be examined in more details in a successive section. The cooling down evolution of the surface is not well visualized with the chosen frame rate since it is a fast phenomenon requiring much higher frame rate [19]. As already specified, herein the attention is mostly devoted to the damage extension linked to the warm area, which is well visualized with the chosen frame rate without any unnecessary overloading of the computer memory.

### 3.1. $\Delta T$ -time plots

To get quantitative information, the  $\Delta T$  images coming from Eq. (1) are then restored to remove temporal noise through subtraction of the average  $\Delta T_{RN}$  signal, which is recorded at the same time over the reference specimen [20]; therefore a corrected  $\Delta T_C$ :

$$\Delta T_C(i, j, t) = \Delta T(i, j, t) - \Delta T_{RN}(t) \quad (2)$$

sequence of images is obtained. Then,  $\Delta T_C$ -time plots are extracted (over the impacted area) and plotted in the following Figs. 5-7. More specifically, maxima values are extracted over a region sufficiently wide of each image, to include the overall impact-affected area. Figs. 5 and 6 display the  $\Delta T_C$  distribution at three impact energies (5, 9 and 15 J), while Fig. 6 shows a comparison between  $\Delta T_C$  plots at  $E = 9$  J of the two specimens.

Looking at Figs. 5-7, two main aspects come out:

- $\Delta T_C$  increases with the impact energy for both specimens (Figs. 5 and 6);
- $\Delta T_C$  is systematically higher for the PC2B specimen as better displayed by the direct comparison of Fig. 7.

The first aspect seems quite normal even if some differences exist in comparison with data obtained in a previous work involving glass-polypropylene specimens [21]. In fact, data of ref [21] displayed a  $\Delta T_C$  reduction increasing the impact energy from 10 to 15 J. This effect has been associated with a local thinning of the material while bending under the pushing impactor force. In other words, the basalt reinforced polypropylene is, in general, unlike the type of interface bond, more rigid (less deformable) than the glass reinforced one and reacts differently to the impact.

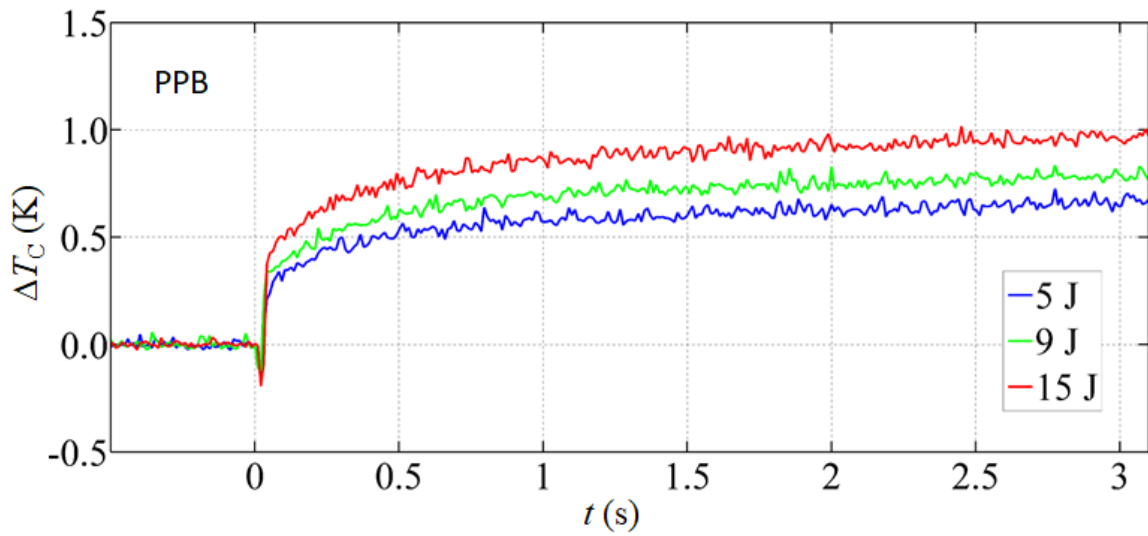


Fig. 5  $\Delta T_C$ -time plots of PPB specimen for varying the impact energy

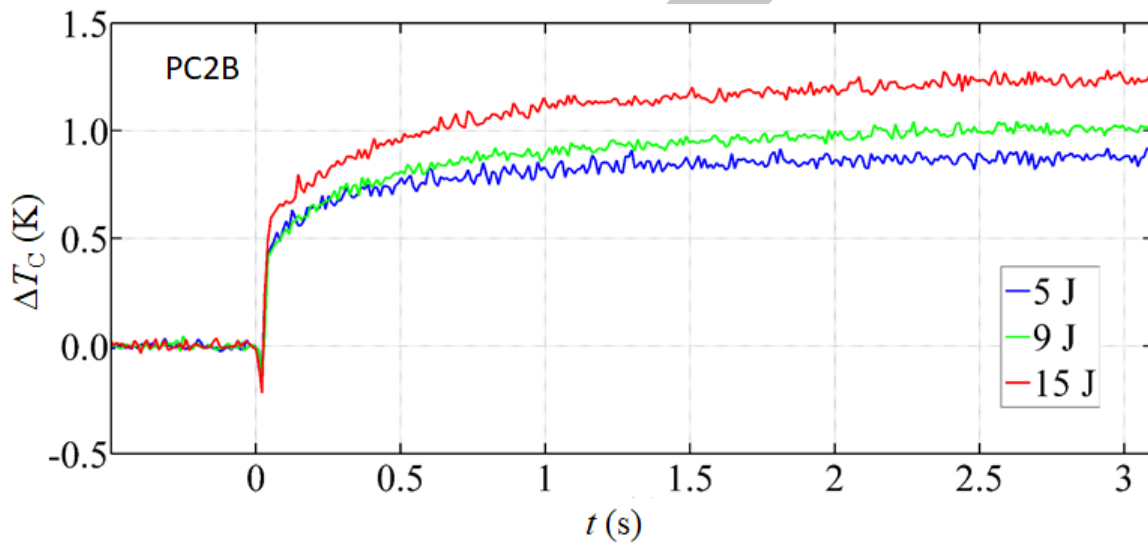


Fig. 6  $\Delta T_C$ -time plots of PC2B specimen for varying the impact energy

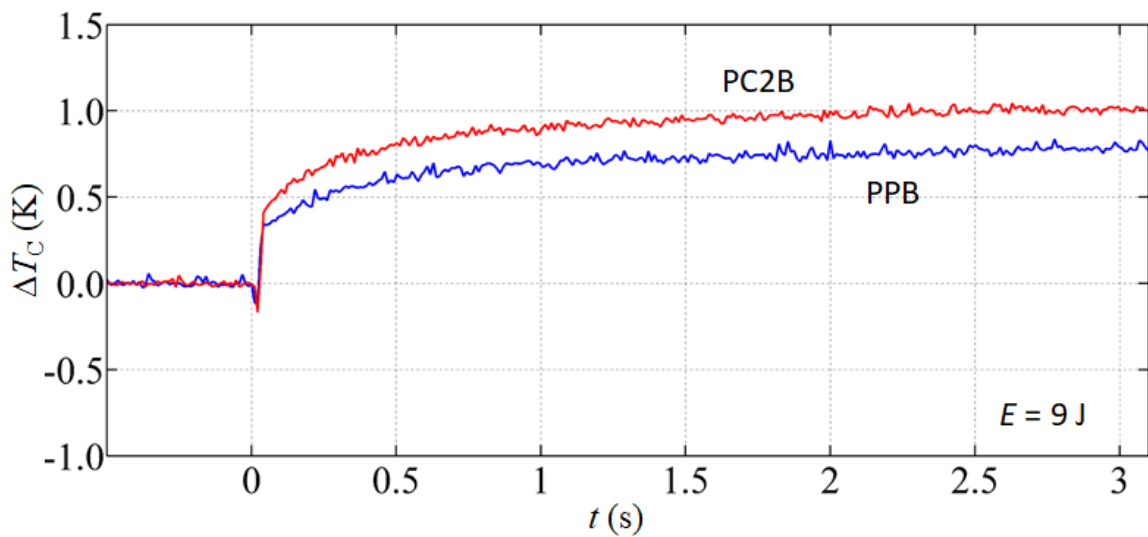


Fig. 7  $\Delta T_C$ -time plots at  $E = 9$  J; a comparison between specimens

The second aspect accounts for the improved fibre-matrix interface strength entailed by the addition of the coupling agent. In fact, since stress is transferred between matrix and fibres across the interface, interfacial bonding plays a key role in the material behaviour. Under the pushing force, a laminate with a weak interface bond may experience shear stresses with matrix fibres debonding, fibres pull-out and delamination. Instead, a stronger interface may preclude slipping of fibres promoting dissipative phenomena with temperature rise.

### 3.2. Damage extension from warm area

The corrected  $\Delta T_C$  sequences of images are used for quantitative measurement of the resulting warm area, which is intended to account for the impact damage extension. In particular, the correspondence between the warm area and the damaged area was already proved with translucent glass/epoxy specimens. In addition in a comparative study [22], the advantage of referring to inline visualization instead of post-impact non-destructive evaluation has also been established.

The measurement of the warm area is done by applying the noise correction reference (NCR) method, which is wholly described in ref [20] with the evaluation of the involved characteristic time. The warm-area contoured images for the two specimens are shown in Fig. 8.

The first thing that jumps to eyes is the enlargement of the warm area with increasing the impact energy and this can be easily assumed as a normal behaviour since one expects a larger damaged area to be caused by a stronger impact. However at a closer look, it comes out that the total warm area is not only generated by the impact energy in itself, but also by secondary effects. In fact, for  $E = 5$  J a central warm area becomes contoured accounting for the damage generated by the impactor nose. But, as the impact energy rises to  $E = 9$  J, the specimen undergoes larger bending being pushed against the edges of the fixture window's shorter side (the window is rectangular). This effect can be easily accounted for by the hotter vertical line on the right side of Fig. 8d (PC2B specimen at  $E = 9$  J), which marks the boundary of the specimen with the metal window's edge. This effect is more pronounced for the PPB specimen (Fig. 8c), but it is less distinguishable and could be confused with the heating generated by damage due to the impactor. Indeed as already observed, the weaker bonding between the superimposed layers of the PPB specimen allows for mutual slipping of layers and larger deformation.

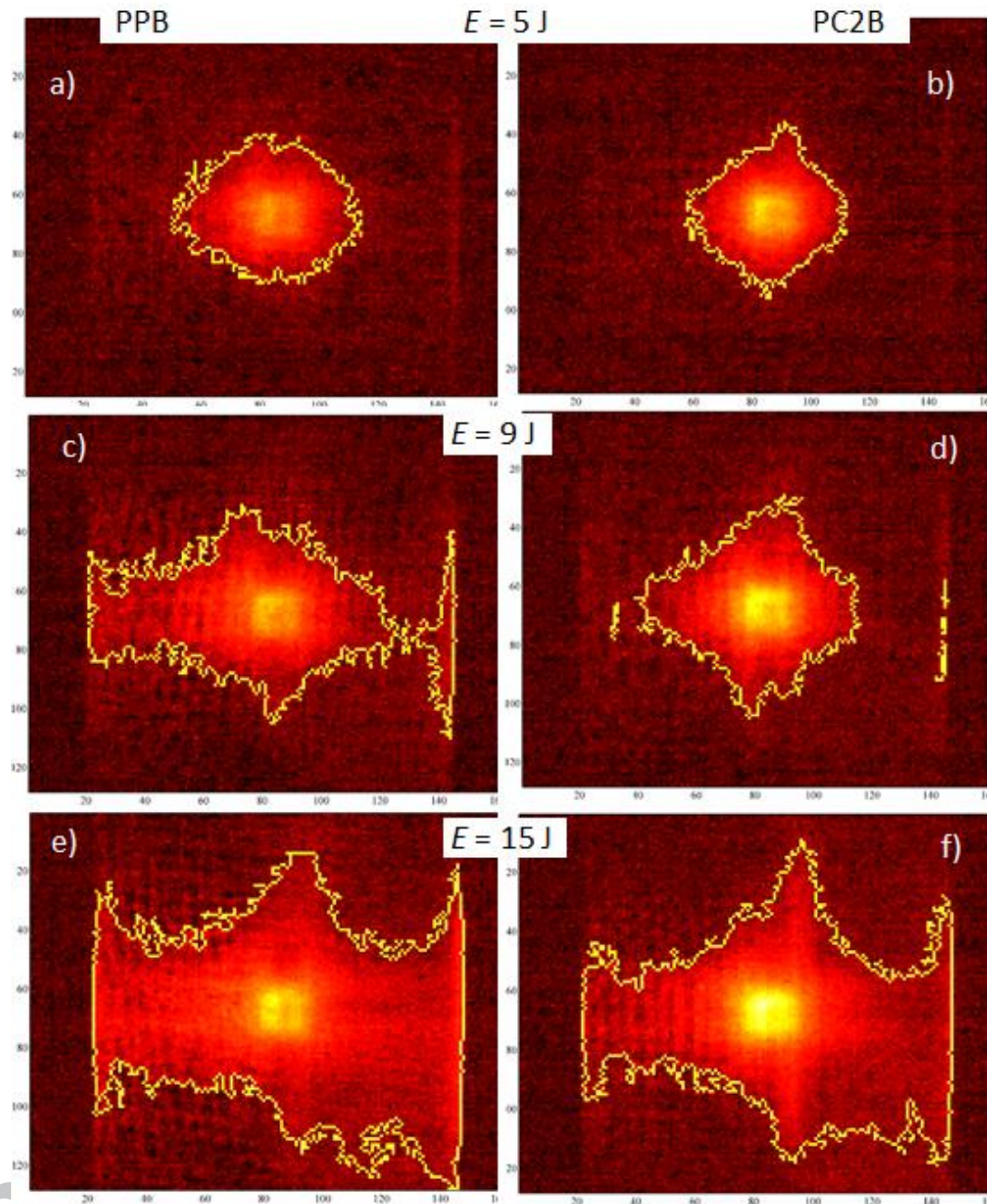


Fig. 8 Contoured warm area with varying the impact energy

At the highest energy of 15 J, both specimens undergo large deformations beyond the space allowed by the window (in the horizontal direction) and for both it is no more possible a definite separation between the heating due to the primary impact (impactor percussion) and that caused by the slamming against the window edges. To better depict the influence of the fixture, the distribution of  $\Delta T_C$  along  $x$  and  $y$  axes, centred at the impact point (Fig. 9), is extracted, for several different time instants, and reported in Fig. 10 for the PPB specimen.

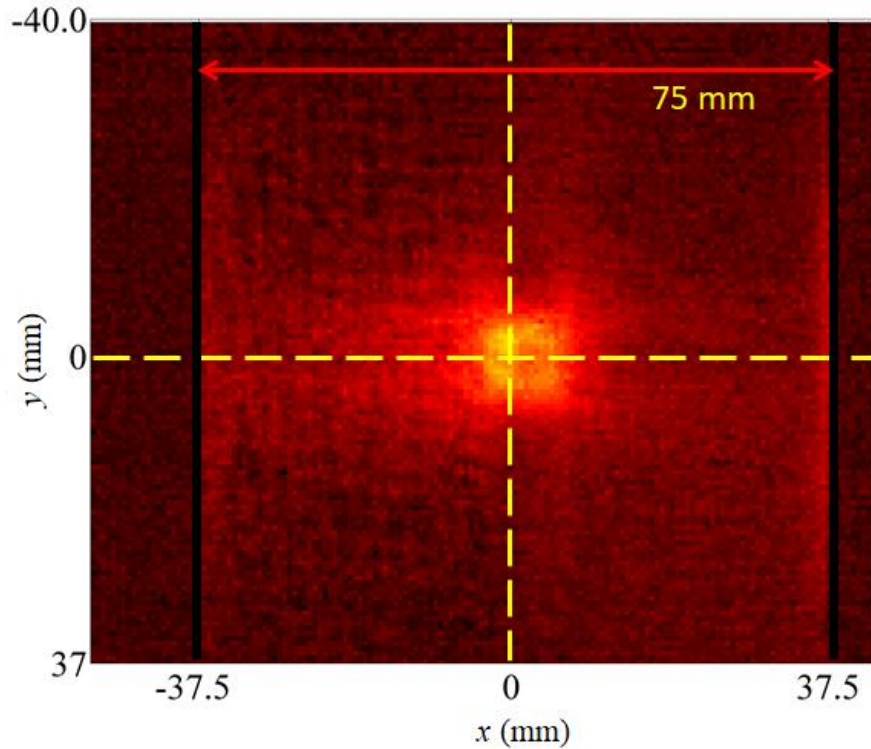


Fig. 9 Schematic representation of  $\Delta T_C$  distribution along  $x$  and  $y$  axes within the window width

As can be seen, the  $\Delta T_C$  distribution along  $y$  takes its maximum in the centre (impact point) and decreases moving away in a quasi-bell shaped fashion. Conversely, the  $\Delta T_C$  distribution along  $x$  is disrupted by an abnormal increase nearby the window border at 37.5 mm (Fig. 9). Indeed, the impact-like damage caused by the pushing against the window border is accompanied by temperature rise with a one-side quasi-bell shape (the specimen continues under the fixture); as expected, this effect becomes stronger with increasing the impact energy. Such effect could be separated from the whole warm area by drawing an interpolation curve connecting the maximum  $\Delta T_C$  with  $\Delta T_C = 0$  in  $\Delta T_C$  plots along  $x$ . This operation may be facilitated by comparing the  $\Delta T_C$  distributions along  $x$  with those along  $y$ ; an example is supplied in Fig. 11 in which one  $\Delta T_C$  distribution along  $y$  is superimposed to the one along  $x$  for  $E = 15$  J for  $t = 1.09$  s. As can be seen, the effect of the window border on the  $\Delta T_C$  distribution along  $x$  is well highlighted.

For a comparison between the two specimens,  $\Delta T_C$  distributions along  $x$  and  $y$  at  $t = 1.09$  s for  $E = 9$  J are shown in Fig. 12. As can be seen along  $y$ , the PC2B specimen displays higher  $\Delta T_C$  values in the central part within the impact point, while, going far away, the  $\Delta T_C$  distributions are practically superimposed. Instead, some differences exist along the  $x$  direction where the PC2B specimen displays again higher  $\Delta T_C$  values in the central part within the impact point, but, going far away, the PPB specimen exhibits higher values, being pushed against the fixture window edge.

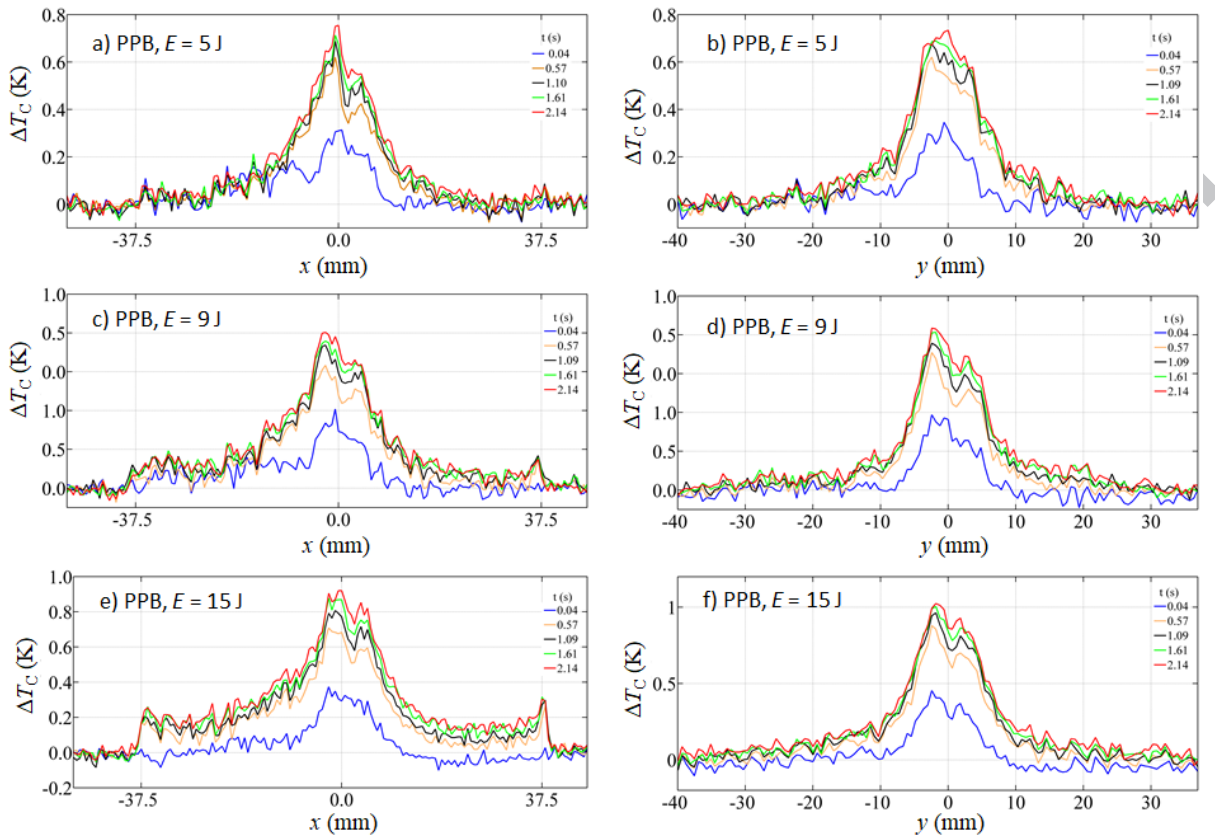


Fig. 10  $\Delta T_C$  distribution along  $x$  (left) and  $y$  (right) axes of the PPB specimen for the three impact energy values

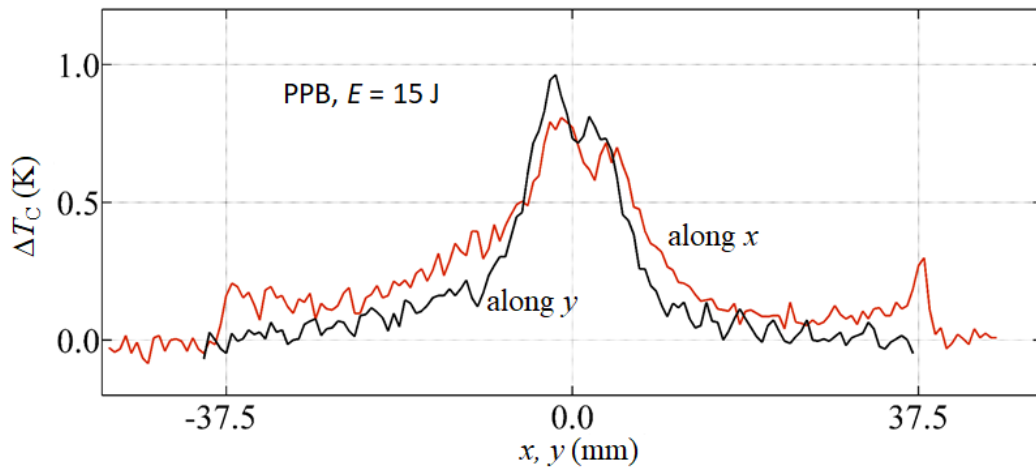


Fig. 11 Comparison between  $\Delta T_C$  along  $x$  and  $y$  axes at  $t = 1.09$  s of the PPB specimen for  $E = 15$  J

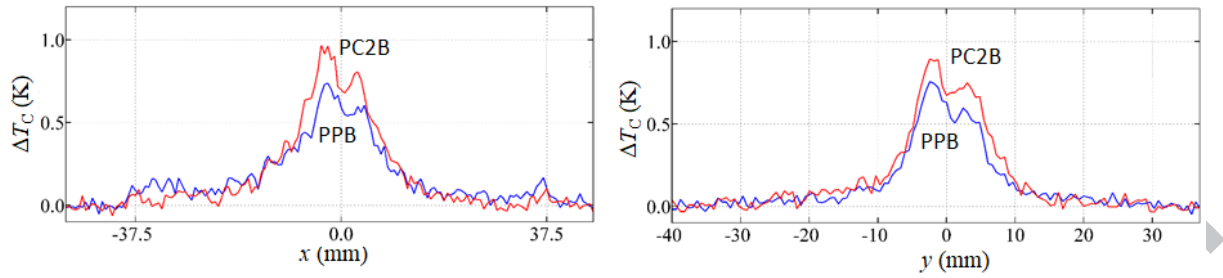


Fig. 12  $\Delta T_C$  along  $x$  and  $y$  at  $t = 1.09$  s for  $E = 9$  J; a comparison between specimens

### 3.3. Comparison with polypropylene/glass composites data

Based on our experience on inline monitoring of impact tests with infrared thermography and going through data, which were collected over the last few years with different types of composites and with the same testing configuration (Charpy pendulum, fixture, etc.) [23], no similar fixture dependent effects are found. The investigated materials involve both thermoset and thermoplastic matrices reinforced with different types of fibres and different stacking sequences. Amongst them, there are some specimens which involve almost the same matrix (a type of polypropylene), stacking sequence and thickness of the present paper and were also impacted at almost the same impact energies.

Therefore, we can compare data obtained with two sets of specimens, which differ only for the reinforcement. Fig. 13 shows the distribution of  $\Delta T_C$  along  $x$  of specimens made of woven glass fibres embedded in a polypropylene matrix and impacted at 8.3 J. In particular, one type of specimens includes a pure polypropylene matrix (PPG), while the other one (PC2G) a polypropylene modified with the addition of 2% of PP-g-MA. As can be seen, for both types of specimens and for both impact energies,  $\Delta T_C$  maintains an almost flat and equal to zero distribution for a quite long tract from the window edge ( $x = 37.4$  mm) moving towards the impact point. A comparison between the  $\Delta T_C$  distribution along  $x$  at two impact energies of 8.3 and 11.6 J of the PPG specimen is shown in Fig. 14. As can be seen, by increasing the impact energy, only a  $\Delta T_C$  increase in the impact point and nearby to it can be observed without any interference with the fixture window edge. This means that there is no interference with the fixture window edge when the polypropylene matrix either pure, or modified with a grafting agent, is reinforced with glass fibres.

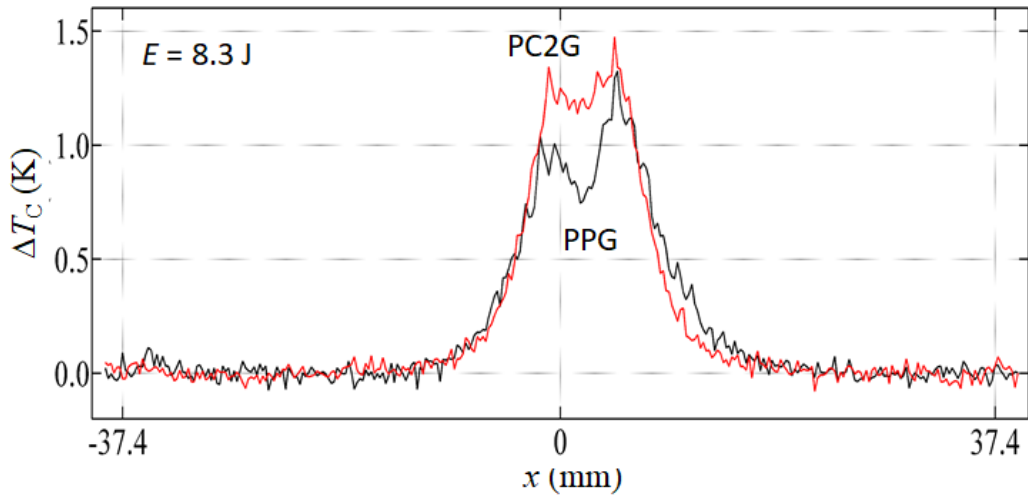


Fig. 13  $\Delta T_C$  along  $x$  at  $t = 1.6$  s for  $E = 8.3$  J; a comparison between specimens PPG and PC2G

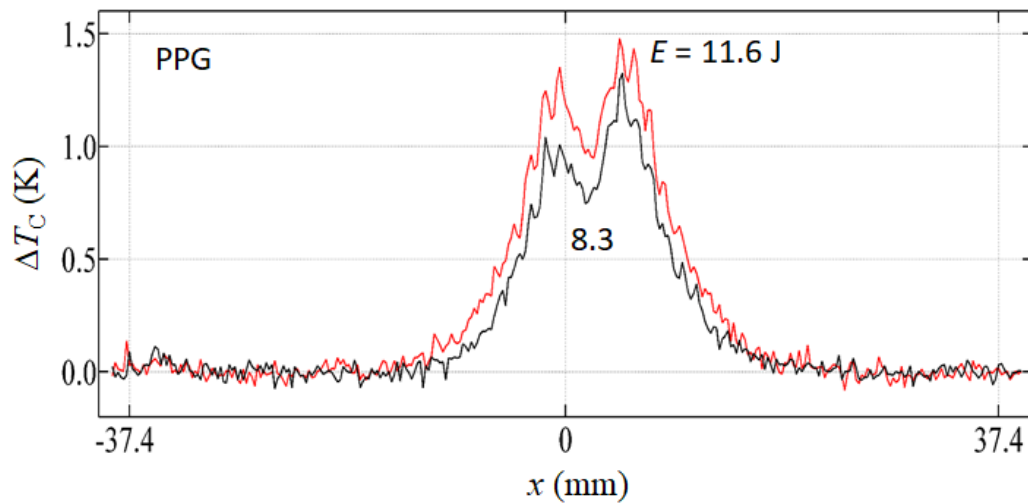


Fig. 14  $\Delta T_C$  along  $x$  at  $t = 1.6$  s of the PPG specimen; a comparison between impact energies  $E = 8.3$  J and  $11.6$  J

#### 4. Conclusions

The presented results bring evidence of two main aspects:

- the behaviour of basalt-based composites under impact;
- the influence of the specimen's fixture on the damage extension.

With regard to the first aspect, it has been observed that the improved matrix/fibres interface strength entails a reduction of the impact affected zone, but with higher dissipation of energy within the impact point; this is in general agreement with previous data on glass/polypropylene composites. Conversely, by increasing the impact energy from 9 J to 15 J, the large material deformation (concavity on the impact side and protrusion on the opposite one) with local thinning it

is not observed; basalt fibres make the resulting composite more rigid and unable to undergo large deformations.

The second aspect, was not observed before on different types of composites (involving also a polypropylene matrix, but reinforced with glass fibres) even if impacted with the same Charpy pendulum and using the same fixture. Of course, this represents an important issue with double meaning. On one side, it focuses attention on the role of the fixture on the impact damaging of materials; the fixture has to be tailored for the specific material. On the other side, and most important, it shows that inline monitoring of impact tests with an infrared camera allows to visualize not only the impact damaging in time, but also any secondary effect, which could contribute to the damage extension and not otherwise being recognisable.

However, further tests are necessary with a more wide variation of parameters to fully ascertain the behaviour under impact of basalt based composites and to shed light on other likely unknown aspects.

## References

1. V. Fiore, T. Scalici, G. Di Bella, A. Valenza, A review on basalt fibre and its composites, *Composites Part B*, **74**, 2015, 74-94.
2. V. Lopresto, C. Leone, I. De Iorio, Mechanical characterisation of basalt fibre reinforced plastic, *Composites Part B*, **42**, 2011, 717-723.
3. I.D.G. Ary Subagia, Y. Kim, L.D. Tijing, C.S. Kim, H.K. Shon. Effect of stacking sequence on the flexural properties of hybrid composites reinforced with carbon and basalt fibers. *Composites Part B*, **58**, 2014, 251-258.
4. L. Hollaway. Polymer composites for civil and structural engineering. New York: Springer; 1993.
5. P.D.L.R. Garcia, A.C. Escamilla, M.N.G. Garcia, Bending reinforcement of timber beams with composite carbon fiber and basalt fiber materials. *Composites Part B*, **55**, 2013, 528-536.
6. F. Sarasini, J. Tirillò, M. Valente, T. Valente, S. Cioffi, S. Iannace, and L. Sorrentino, Effect of basalt fiber hybridization on the impact behavior under low impact velocity of glass/basalt woven fabric/epoxy resin composites, *Composites Part A*, **47**, 2013, 109-123.
7. R.V. Subramanian, Basalt Fiber - A New Cost Mineral Fiber For Composites. Advanced Composites Technology - Conference on Advanced Composite Technology, 1978.
8. S.E. Artemenko, Polymer Composite Materials Made From Carbon, Basalt, And Glass Fibers. Structure and Properties. *Fiber Chemistry*, **35**, 2003, 226-229.

9. K. Van de Velde, P. Kiekens, L. Van Langenhove, 'Basalt Fibers As Reinforcement For Composites', <http://www.basaltex.com/logos/basalt%20fibres.pdf>, accessed on September 2018.
10. Basaltex, The thread of stone, <http://www.basaltex.com>, accessed on September 2018.
11. O.O. Medvedyev, Y.L. Tsybulya, The Outlook for the use of basalt continuous fibers for composite reinforcement. International SAMPE Symposium and Exhibition, **49**, 2004. 2299-2303.
12. V.P. Sergeev, Y.N. Chuvashov, O.V. Galushchak, I.G. Pervak, I. G., N.S. Fatikova, Basalt Fibers - A Reinforcing Filler for Composites. Power Metallurgy and Metal Ceramics, **33**, 1994. 555-557.
13. M. Botev, H. Betchev, D. Bikiaris, C. Panayiotou, Mechanical Properties and Viscoelastic Behavior of Basalt Fiber-Reinforced Polypropylene, *J Appl Polym Sci* **74**, 1999, 523–531.
14. M.T. Kim, K.Y. Rhee, H.J. Kim, D.H. Jung, Effect of moisture absorption on the flexural properties of basalt/CNT/epoxy composites. *Carbon Lett*, **13**, 2012, 187–189.
15. V. Dhand, G. Mittal, K.Y. Rhee, S.J. Park, D. Hui, A short review on basalt fiber reinforced polymer composites, *Composites B*, **73**, 2015, 166-180.
16. C. Meola, S. Boccardi, G.M. Carlomagno, Infrared thermography in the evaluation of aerospace composite materials, Woodhead Publishing Print Book ISBN :9781782421719, 180 pages, 2016.
17. W. Thomson, On the thermoelastic, thermomagnetic and pyroelectric properties of matters, *Philosophical Magazine*, 1978; 5: 4-27.
18. M.A. Biot, Thermoelasticity and irreversible thermodynamics *Journal of Applied Physics*, **27**, 1956, 240-253.
19. C. Meola, S. Boccardi, N.D. Boffa, F. Ricci, G. Simeoli, P. Russo, G.M. Carlomagno, New perspectives on impact damaging of thermoset- and thermoplastic-matrix composites from thermographic images, *Composite Structures*, **152**, 2016, 746-754.
20. S. Boccardi, G.M. Carlomagno, C. Meola, Post-processing of time-sequences acquired during impact tests with the aid of a reference area, in Proc. QIRT 2016, 4-8 July 2016, Gdansk, Poland, paper n.10, (9 pages).
21. S. Boccardi, G.M. Carlomagno, G. Simeoli, P. Russo, C. Meola, Evaluation of impact affected areas of glass fibres thermoplastic composites from thermographic images, *Measurement Science and Technology*, **27**, 2016, 075602 (12pp).

22. C. Meola, S. Boccardi, G.M. Carlomagno, N.D. Boffa, E. Monaco, F. Ricci, Nondestructive evaluation of carbon fibre reinforced composites with infrared thermography and ultrasonics, *Composite Structures*, **134**, 2015, 845-853.
23. S. Boccardi, Infrared thermography to monitoring mechanical tests on composite materials: Experimental procedure and data analysis, PhD Thesis, 2017.